Robotics and Autonomous Systems 61 (2013) 626–636

Contents lists available at SciVerse ScienceDirect

Robotics and Autonomous Systems

journal homepage: www.elsevier.com/locate/robot

Multi-fingered grasp synthesis based on the object dynamic properties☆

V. Lippiello *, B. Siciliano, L. Villani

PRISMA Lab, Dipartimento di Ingegneria Elettrica e Tecnologie dell'Informazione, Università degli Studi di Napoli Federico II, Via Claudio 21, 80125 Napoli, Italy

HIGHLIGHTS

- We propose a new approach to quickly synthesize an optimal *n*-fingered grasp.
- Minimization of gravitational and inertial effects are ensured.
- Both 2D and 3D complex of any shape object can be considered.
- The proposed approach is useful for the manipulation of heavy objects.
- Several case studies and comparisons with other methods are presented.

ARTICLE INFO

Article history:
Received 2 August 2012
Received in revised form
24 January 2013
Accepted 1 February 2013
Available online 26 February 2013

Keywords:
Grasp synthesis
Grasping
Multi-fingered hands

ABSTRACT

The grasping and manipulation of objects, especially when they are heavy with respect to the hand power capability, requires the synthesis of grasp configurations that explicitly take into account the dynamic properties of the object. Specifically, suitable grasp configurations reducing gravitational and inertial effects during object manipulation, and minimizing and equally distributing the grasping forces among all the available fingers, must be computed. A new method for fast synthesis of multi-fingered grasp configurations is proposed in this paper. In particular, to reduce the computational complexity, all the regions of the object surface favoring the synthesis of minimal inertia grasps are evaluated first. Then, a reduced number of discrete grasping regions are selected on the basis of the fingertip size, model uncertainty, and surface curvature. Finally, an exhaustive search of the optimal grasp configurations with respect to the grasp quality is performed. Several case studies and comparisons with other methods are proposed to demonstrate the effectiveness of the proposed approach.

1. Introduction

The manipulation of an object requires at least the capability of the robotic hand to guarantee a firm grasp. The weight and inertia of heavy objects may severely influence the *stability* [1] and the *disturbance resistance* capability [2] of the grasp, as well as the *dexterity* [3,4] during motion, in view of the joint torque limits of the robotic hand [5,6]. An inadequate grasp configuration could require to spend a large part of the available torques, thus limiting the manipulability. Therefore, grasp synthesis must explicitly take into account these factors.

Another relevant aspect in grasp synthesis is the desired task that has to be executed after the grasp. In [7] optimal grasp points on an arbitrary-shaped grasped object using a required external force set has been investigated. In detail, the required external force set is given based on a task, and consists of the external forces and moments, which must be balanced by virtue of contact forces applied by a robotic hand. In [8] the intended task has been employed as a discriminatory factor in the choice of the best grasp configuration within a set of candidates provided by a large database of human grasp observation.

Robot grasp synthesis algorithms have been reviewed in [9], but since then important progress has been made toward applying learning techniques to the grasping problem. An overview that presents computational algorithms for generating 3D object grasps with autonomous multi-fingered robotic hands is proposed in [10], with a focus on analytical as well as empirical grasp synthesis approaches, and more in general in [11]. In [12] an approach toward planning robot grasps across similar objects by part correspondence is presented. The novelty of this method lies in the topological decomposition of objects that enables high-level semantic grasp planning. A method for the online grasp planning of unknown objects with a multi-fingered robotic hand has been presented in [13,14]. The algorithm is composed of a visual object-surface reconstruction algorithm and a local grasp planner that evolve in parallel.

☆ The research leading to these results has been supported by the ARCAS Large-scale integrating project, which has received funding from the European Community's Seventh Framework Programme (FP7/2007-2013) under grant agreement ICT-287617. The authors are solely responsible for its content. It does not represent the opinion of the European Community and the Community is not responsible for any use that might be made of the information contained therein.

* Corresponding author. Tel.: +39 0817683635.
E-mail addresses: vincenzo.lippiello@unina.it (V. Lippiello), bruno.siciliano@unina.it (B. Siciliano), luigi.villani@unina.it (L. Villani).

0921-8890/$ – see front matter © 2013 Elsevier B.V. All rights reserved.
http://dx.doi.org/10.1016/j.robot.2013.02.003

The off-line computation of a context-independent (only the robot hand and the object to grasp are considered) and dense set of grasps, instead of a small set of grasps regarded as optimal with respect to a given criterion, are considered in [15]. This set is then used on-line to let the robot quickly choose a grasp adapted to a specific situation.

Many methods have been proposed so far for the synthesis of optimal grasp configurations based on the combination of different grasp quality indices. A wide collection of quality measures can be found in [16], while a more general overview of grasping is proposed in [17]. The problem of combining indices with different physical meaning is addressed in [18,19], where several non-dimensional performance indices are proposed. In [20] the manipulation task that has to be executed is suitably modeled and considered as a quality measure for the grasp synthesis using dexterous hands.

Most of the proposed approaches make use of combinations of different grasp quality indices to achieve a global quality measure to rank all possible grasps either in a *parallel* or in a *serial* way. The parallel approach combines different quality indices into a global one. Considering that all of them have to be either maximized or minimized, the algebraic (weighted) sum of the quality indices can be considered [21]. With the serial approach, a significant grasp quality measure (or a suitable combination) is employed to generate candidate grasp configurations. Then, the best candidate is chosen using a secondary quality measure (or a suitable combination), resulting in a prioritized synthesis criterion [22].

Both these approaches have pros and cons. The results of the parallel approach strongly depend on the weights assigned to each index and the importance of the single measure is confused into the resulting global measure. On the other hand, with the serial approach, the synthesized grasps strongly depend on the thresholds and on the priority order employed to discriminate the grasp candidates, often resulting in unstable algorithms—little changes in the shape of the object or in the threshold may determine the choice of a completely different set of grasps.

Another significant aspect to consider is the computational complexity of the optimal grasp search algorithms. From this point of view, indeed, the case of polyhedral objects is one of the most investigated. The reason is that the evaluation of the force-closure regions can be reduced to a computationally efficient linear programming problem [23,24], while the best grasp can be computed by solving a nonlinear programming problem [25]. The problem is further simplified if only planar grasps are considered [26].

For the most general case of grasp synthesis (not necessary planar) for 3D objects with n-fingers, the complexity of most of the available algorithms rapidly becomes untractable. For those cases, often the object is locally approximated with planar surfaces [21], sometimes holding additional aggregated information on discretized regions, e.g. region curvature. In [27] a geometrical approach to compute force closure grasps, with or without friction and with any number of fingers, is presented. In detail, the object's surface is discretized in a cloud of points, and thus the algorithm is applicable to objects of any arbitrary shape.

The synthesis of multi-fingered grasps with a realistic representation of the contact between the fingers of a robotic hand and an object has been proposed in [28]. A patch contact model has been employed to approximate the contact between a rigid object and a deformable anthropomorphic finger as a set of Independent Contact Regions (ICRs).

In this paper, an extension of the work presented in [29] is proposed to quickly synthesize an optimal n-fingered grasp configuration for 2D/3D complex objects ensuring the minimization of gravitational and inertial effects. To reduce the complexity of the problem, the discretization of the object surface is performed. However, differently from the existing approaches, this process is made under constraints derived from significant grasp measures, resulting in a drastic reduction of the computational complexity. In particular, the proposed method requires first the evaluation of object surface regions that can generate grasps with minimal gravitational and inertial effects. The resulting regions are further divided on the basis of the local curvature, resulting in a set of regions with a uniform curvature (e.g. concave regions, planar regions, convex regions, and angular regions). This allows privileging the grasp on concave regions, which are more stable [30]. The resulting regions are further decomposed also considering the fingertip size and the object model uncertainty. Finally, a set of grasp measures is applied in a prioritized order to rank all the possible grasp configurations according to a serial approach, which also takes into account the computational complexity of the employed indices.

Several case studies and comparisons with other methods are presented. In view of the choice of the first quality metric, the proposed approach is useful especially for the manipulation of heavy objects, compared to the hand capabilities.

2. Object surface discretization

Complex objects with curved surfaces that cannot be approximated with a polyhedral need to be discretized to reduce the complexity of the optimal grasp search algorithm. A new approach based on the direct use of grasp measures for the selection and the discretization of the object surface into connected regions is proposed in the following.

2.1. Minimal inertia regions

The first criterion for regions selection adopted in this work is the minimization of the grasp forces required to compensate for gravitational and inertial forces. Typically, this objective is achieved by minimizing the distance between the center of mass of the object and the center of grip [21,23], defined as the centroid of the polyhedron with the contact points as vertices [31]. This criterion, however, takes into account only the positions of the contact points and not the orientation of the lines of action of the contact forces.

It is easy to recognize that the "ideal" situation to cope with gravity and inertial forces is fulfilled when the lines of action of the contact forces have an isotropic angular distribution and intersect in the object center of mass. In [21,32] these criteria are referred as "Focus Centering" and "Force Arrangement", as a criteria for the grasp assessment, and "Real Focus Centering", as a criteria for the configuration assessment. Starting from these assumptions – in the case of hard fingers and point contact with friction – if the friction cones in the points of contact contain the object center of mass, then the resulting center of grasp has to remain close to the center of a favorable condition to obtain stable grips with respect to wrenches generated by gravitational and inertial forces.

In view of the above considerations, the "minimal-inertia regions" are defined as those parts of the object surface where, for a given friction coefficient μ, the corresponding friction cone contains the object center of mass $\boldsymbol{c}_m$.

Assuming that a representation of the object surface $\mathcal{S}$ is known (e.g. extracted from a CAD model or constructed with a visual system or a direct tactile inspection), a finite set of minimal-inertia regions $\mathcal{R}_I = \{\mathcal{R}_{I1}, \ldots, \mathcal{R}_{Ii}\}$ can be defined as the set of all the connected subsets $\mathcal{R}_{Ik}$ of $\mathcal{S}$ such that

$$\forall \boldsymbol{p} \in \mathcal{R}_I, \quad \boldsymbol{n}^{\mathrm{T}}(\boldsymbol{p})\boldsymbol{c}(\boldsymbol{p}) \leq \cos(\arctan(\mu)), \tag{1}$$

where $\boldsymbol{n}(\boldsymbol{p})$ is the inward unit vector normal to the object surface at the contact point $\boldsymbol{p}$ and $\boldsymbol{c}(\boldsymbol{p})$ is the *central vector*, defined as the unit vector pointing from $\boldsymbol{p}$ to $\boldsymbol{c}_m$ (see Fig. 1).

Fig. 2 shows the 3D CAD model of a duck-toy (on the left) and the corresponding minimal-inertia regions for a given friction coefficient μ (in yellow on the right). The center of gravity of the object is shown with a black sphere.

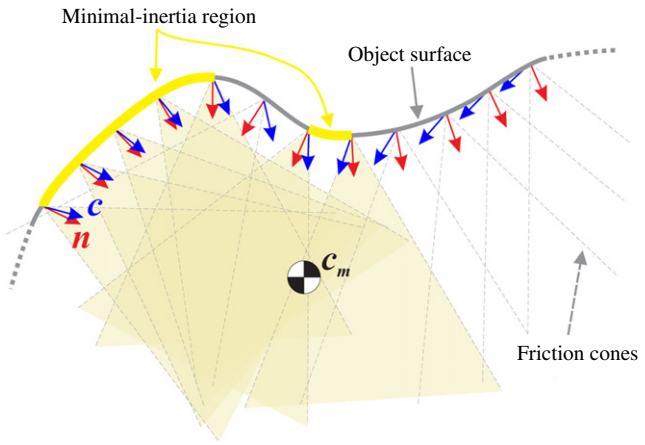

Fig. 1. Minimal-inertia regions (in yellow) for a piece of an object surface (in gray). (For interpretation of the references to colour in this figure legend, the reader is referred to the web version of this article.)

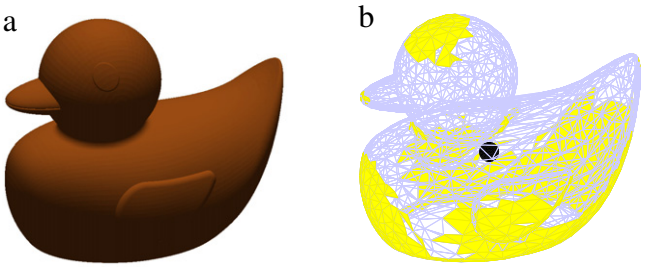

Fig. 2. A 3D duck-toy model (on the left) and the corresponding minimal-inertia regions (in yellow on the right). (For interpretation of the references to colour in this figure legend, the reader is referred to the web version of this article.)

By restricting the evaluation of the grasp configurations only to the regions in $\mathcal{R}_I$, the gravitational and inertial effects will be reduced. Moreover, having discarded pieces of the object surface, the computational complexity of the grasp search algorithm will be reduced, too. Notice that the decomposition $\mathcal{R}_I$ depends on the friction coefficient μ used for regions selection.

2.2. Uniform curvature regions

Each region of $\mathcal{R}_I$ is further divided into smaller connected regions with uniform curvature, resulting in a new set of regions named uniform curvature regions $\mathcal{R}_C = \{\mathcal{R}_{C1}, \ldots, \mathcal{R}_{Cu}\}$. Considering two unit vectors $\boldsymbol{t}(\boldsymbol{p})$ (known as the tangent unit vector) and $\boldsymbol{b}(\boldsymbol{p})$ (known as the bi-normal unit vector), which are orthogonal to each other and to the inward normal unit vector $\boldsymbol{n}(\boldsymbol{p})$, the *curvature matrix* of the object surface at a point $\boldsymbol{p}$ is the symmetric 2×2 matrix

$$\boldsymbol{K}(\boldsymbol{p}) = \begin{bmatrix} \dfrac{\partial^2 \boldsymbol{n}(\boldsymbol{p})}{\partial^2 \boldsymbol{t}} & \dfrac{\partial^2 \boldsymbol{n}(\boldsymbol{p})}{\partial \boldsymbol{t} \partial \boldsymbol{b}} \\ \dfrac{\partial^2 \boldsymbol{n}(\boldsymbol{p})}{\partial \boldsymbol{b} \partial \boldsymbol{t}} & \dfrac{\partial^2 \boldsymbol{n}(\boldsymbol{p})}{\partial^2 \boldsymbol{b}} \end{bmatrix}. \tag{2}$$

The eigenvalues of this matrix are denoted as *principal curvatures* and are real numbers due to the matrix symmetry.

By denoting with $k(\boldsymbol{p}) \in [-1, 1]$ the ratio between the minimum and maximum eigenvalue of $\boldsymbol{K}$ – taken positive if the surface is locally on the same side of the osculating plane as $\boldsymbol{n}$ and negative otherwise – the regions of $\mathcal{R}_I$ are divided into smaller connected regions on the basis of similar values of k. Notice that, $k(\boldsymbol{p})$ represents a measure of the local curvature of the surface in the point $\boldsymbol{p}$, therefore low values of k correspond to almost planar surfaces,

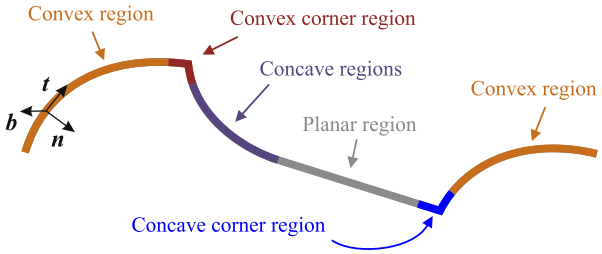

Fig. 3. Uniform curvature regions represented on a piece of an object surface.

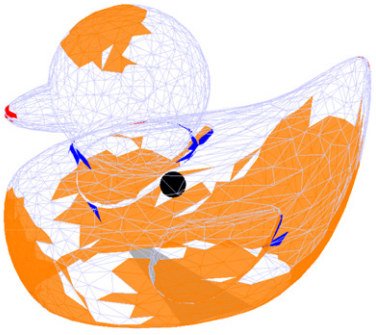

Fig. 4. Uniform curvature regions of the duck-toy shown in Fig. 2.

while high values corresponds to corners (angular regions). If a discrete representation of the object surface is available, e.g., triangle mesh, $k(\boldsymbol{p})$ represents the maximum curvature among the surface containing $\boldsymbol{p}$ and the adjacent ones. Hence, each minimal inertia region can be split into a number of five types of regions: (1) planar region, if $|k| \leq k_p$; (2) convex region, if $k_p < k < k_a$; (3) convex corner region, if $k \geq k_a$; (4) concave region, if $-k_a < k < -k_p$; (5) concave corner region, if $k \leq -k_a$ (see Fig. 3). A 3D example of uniform curvature regions is shown in Fig. 4, which corresponds to the CAD model of Fig. 2. The quantities k_p and k_a, with $0 < k_p < k_a < 1$, are the thresholds employed to distinguish planar from convex, concave and corner regions, respectively. For example, by assuming that $k_a = 0.8$ ($k_p = 0.05$) a region is considered a convex corner (locally planar) if the difference in the curvature between the current surface and the adjacent ones is higher or equal than 80% (in absolute value less than 5%).

In [30] it was analytically demonstrated how concave regions produce contacts that are more stable than planar and convex ones. Hence, each type of region is ranked differently on the basis of its capability to produce stable contacts. The curvature ranking will be employed during the grasp configuration search as a measure of the contact stability. Specific considerations have to be done for angular regions (regions with a high curvature). Convex angular regions can produce unstable contacts, and thus they should be avoided. On the other hand, convex angular regions can produce stable contacts but the real contact between the fingertip and the object are typically placed in different and unpredictable points, also due to model inaccuracy, resulting in uncertain grasps. For these reasons, angular regions are discarded if other regions are available.

2.3. Grasp regions

The evaluation of the final set of *grasp regions* $\mathcal{R}_G = \{\mathcal{R}_{G1}, \ldots, \mathcal{R}_{Gr}\}$ – the finite set of connected regions on which a safe and stable contact can be achieved – is performed by extracting from each region of $\mathcal{R}_C$ a number of smaller regions, with a size adequate to locate a fingertip, suitably distributed on it. In this paper, grasp regions composed by points with maximum distance $r_g > 0$ from a central point are considered. The parameter r_g can be chosen equal to the mean tip radius.

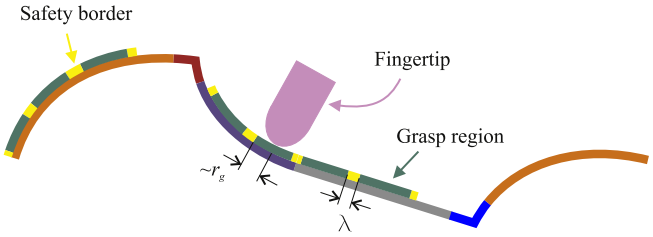

Fig. 5. Graphical representation of the grasp regions (green) and safety borders (yellow) represented on a piece of an object surface discretized on the base of the minimal-inertia and uniform curvature criteria. (For interpretation of the references to colour in this figure legend, the reader is referred to the web version of this article.)

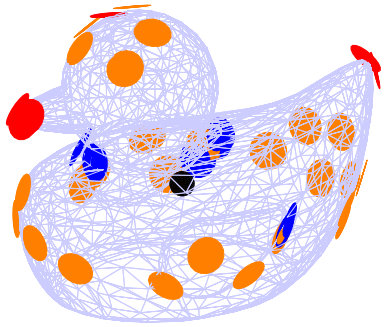

Fig. 6. Grasp regions of the duck-toy shown in Fig. 2.

There are at least two factors influencing the grasp region extraction: the finger size and the accuracy of the model. Considering only these factors, a practical solution may be a uniform distribution of the grasp regions in a way to maximize their number (see Fig. 5). To ensure a safe tip positioning in the presence of model uncertainty, a safety border with a radial dimension $\lambda > 0$ is added to each circular grasp region. Hence, the choice of λ strongly depends on the model uncertainty, i.e. good object models are given a smaller λ and vice versa, however a minimum safety border equal to the 5%–10% of r_g should be considered.

A more effective decomposition can be obtained if a third parameter is considered: the capability to generate normal forces pointing toward the object center of mass $\boldsymbol{c}_m$. In particular, the grasp region selection is performed with the iterative algorithm described below:

1. If the set $\mathcal{R}_C$ contains regions that have not yet been elaborated, one of those regions is set as "processing" region $\mathcal{R}_p$ and the process goes to step 2; otherwise, the process ends.
2. If the area of $\mathcal{R}_p$ is sufficient to instantiate a new grasp region, the process continues with step 3; otherwise, $\mathcal{R}_p$ is discarded and the process goes back to step 1.
3. The point $\boldsymbol{p}_{nc}$ of $\mathcal{R}_p$ that minimizes the angle between the normal vector $\boldsymbol{n}$ and the central vector $\boldsymbol{c}$ is identified, and the minimum distance $d_{\min}$ between $\boldsymbol{p}_{nc}$ and the region borders is evaluated.
4. If $d_{\min} \geq r_g + \lambda$, a new grasp region, centered at $\boldsymbol{p}_{nc}$, is added to $\mathcal{R}_G$ and cut from $\mathcal{R}_p$. Otherwise, if $d_{\min} < r_g + \lambda$, a new grasp region is chosen as close as possible to $\boldsymbol{p}_{nc}$.
5. The process goes back to step 2.

The final number of grasp regions in $\mathcal{R}_G$ depends on the object size with respect to the fingertip size and, obviously, on the object shape. For typical cases, the number of regions may range from 20 to 50; this ensures a good trade-off between quality of the final grasp and computation time. In any case, if required, the number of regions can be reduced by increasing the safety border dimension λ. A 3D example of grasp regions for the duck-toy model of Fig. 2 is shown in Fig. 6, where the color code employed in Fig. 3 has been employed to discriminate the nature of the corresponding uniform curvature region.

3. Optimal grasp evaluation

Once a finite number of grasp regions $\mathcal{R}_G$ is available, the best n-fingered grasp configuration has to be evaluated. This step is performed by adopting different grasp measures in a hierarchical (serial) composition. To reduce the overall computational complexity, the adopted quality indices have been split into two groups. The first group is employed in a hierarchical manner to rank all the possible grasp configurations which can be derived from $\mathcal{R}_G$.

At the completion of the first massive grasp ranking, the second group of measures – with higher computational complexity – is applied, starting from the configuration with the best rank. Hence, all the configurations which do not guarantee a suitable level for properties such as force-closure, manipulability, and hand kinematic constraints are discarded. A short description of the adopted grasp measures and of the priority composition method is presented in the following.

3.1. Angular distribution and minimal inertia index

Different authors have demonstrated that a uniform angular distribution of the grasp points increases the capability of the grasp to resist to external forces or disturbances [21,33]. In addition, if the lines of action of the contact forces point toward the center of mass of the object, also the gravitational and inertial effects are reduced, resulting in a dynamically consistent isotropic grasp. To this purpose, a new composed index to rank the solid-angular distribution of a n-fingered grasp and the capability to reduce the gravitational and inertial effects is defined as follows:

$$I_D = (2\pi/n)^n \prod_{i=1}^{n} \left| \min_{j \neq i} \arccos\left(\boldsymbol{c}_i^{\mathrm{T}} \boldsymbol{c}_j\right) - \arccos\left(\boldsymbol{n}_i^{\mathrm{T}} \boldsymbol{c}_i\right) \right|^{-1}, \tag{3}$$

where $\boldsymbol{n}_i$ is the inward unit vector normal to the object surface at the i-th contact point and $\boldsymbol{c}_i$ is the corresponding central unit vector.

This index tends toward 1 when $\boldsymbol{n}_i$ and $\boldsymbol{c}_i$ are aligned and the central vectors $\boldsymbol{c}_i$ have a uniform (spatial) angular distribution with respect to $\boldsymbol{c}_m$.

3.2. Extension index

The capability of a grasp configuration to resist to external moments increases with the volume of the polyhedron having the grasp points as vertices [34,35]. Therefore, an "extension" index I_E that measures the volume of the polyhedron can be defined. Obviously, in the case of planar grasps, the area of the grasp polygon is considered.

3.3. Curvature index

The curvature index I_C is an integer value evaluated by summing a score assigned to each type of region composing the considered grasp configuration. In particular, the following score is adopted: 0 for concave region, 1 for planar region, 2 for convex region, 5 for convex angular region, 10 for concave angular region. In this way, grasps with an index close to zero have more stable contacts.

3.4. Force-closure test

Force-closure is an essential property of any grasp configuration, because it guarantees that the grasp can resist any external force and moment applied to the object [36]. Typically, grasps with a good value of I_D are more likely to be force-closure grasps. The evaluation of this property is computationally expensive compared to the quality indices presented before. In the proposed approach,

force closure is evaluated only for the grasp configurations selected after the massive first step of ranking, and only for the configurations with the best rank. In this paper, the method proposed in [37] has been used as a force-closure test.

3.5. Grasp isotropy index

To achieve a precise position or force control when an object is being manipulated by multi-fingered hands any finger has to be far from a singular position.

The grasp isotropy index is useful to measure this configuration [16,18], with the aim to possibly obtain a uniform contribution of the contact forces to the total force and moment applied to the object. This is defined as:

$$I_G = \sigma_{\min}(\boldsymbol{G})/\sigma_{\max}(\boldsymbol{G}), \tag{4}$$

where $\boldsymbol{G}$ is the grasp matrix of the considered configuration [36], and $\sigma_{\min}(\boldsymbol{G})$ and $\sigma_{\max}(\boldsymbol{G})$ are the minimum and maximum singular values of $\boldsymbol{G}$. This index is close to 1 when the grasp is isotropic, and goes to zero when the grasp is close to a singular configuration.

3.6. Hand and task kinematic indices

The quality of a grasp also depends on the hand configuration and on the compatibility with respect to the assigned task. In the literature, many quality measures have been proposed, typically based on the analysis of the Jacobian matrix of the system composed by the hand and the object $\boldsymbol{G}^{\dagger\mathrm{T}}\boldsymbol{J}_h$, where $\boldsymbol{G}^{\dagger}$ is the generalized inverse of the grasp matrix, and $\boldsymbol{J}_h$ is the hand Jacobian. Also, some other aspects, such as joint limits and environmental constraints, can be considered [16]. In particular, in this paper a weighted combination of a measure of the distance with respect to a singular configuration and of the configuration manipulability has been considered. In detail, the measure of the distance with respect to a singularity is defined as follows:

$$Q_s = \sigma_{\min}(\boldsymbol{J}_h), \tag{5}$$

that is the smallest singular value of the hand Jacobian matrix (that becomes zero in correspondence of a singularity), while the adopted measure of the manipulability is set as the volume of the manipulability ellipsoid defined as:

$$Q_m = \sqrt{(\det(\boldsymbol{J}_h\boldsymbol{J}_h^{\mathrm{T}}))}. \tag{6}$$

The adoption of a convex sum of these indexes allows discriminating different configurations that have a similar smallest singular value (e.g. when two or more singularities are approached).

Notice that the hand Jacobian matrix depends on the hand joint positions. If no redundancy is present in the hand kinematics, then by imposing a grasp configuration also the joint positions are fixed as well. On the other hand, in case of redundancy, infinite joint configurations are compatible to the assigned grasp configuration. However, in this case, it is always possible to choose the hand pose that maximizes the adopted manipulability indices.

3.7. Grasp ranking and test method

The grasp ranking is performed into two steps. First, an exhaustive massive evaluation of all the feasible grasp configurations from the set $\mathcal{R}_G$ is performed by applying, in a hierarchical order, the angular distribution and minimal inertia index, the extension index, and the curvature index.

Thanks to the adopted dynamic-consistent approach, the resulting number of grasp regions is typically a low number. However, to further reduce the research space without to losing significant grasp configurations, the kinematics of the adopted hand/gripper is employed off-line to define linear constraints that allow to cut off all the grasp regions which are infeasible. In detail, these linear constraints define, in a conservative way, the volume that contains the hand/gripper workspace for an assigned wrist pose. The feasible grasp configurations set is defined by assigning the first finger (for an anthropomorphic hand this is the thumb) to all the computed grasp regions. Hence the defined volume is moved in the space according to the position of the first finger in such a way that the center of gravity of the object remains as close as possible to the center of gravity of the hand workspace. Typically the rotation about the straight line connecting the first finger position with the center of mass of the object can be freely chosen to fix the pose of the volume. In this case, a discrete number of rotations are considered. Finally, by applying these constraints to each grasp region, only a low number of feasible grasp regions remain to be considered for the other fingers. The above procedure allows to considerably speed-up the whole grasp ranking procedure.

Then, this set of feasible n-fingered grasp configuration is inserted into the current Grasp Ranking List (*GRL*) through the following algorithm:

1. All grasp configurations already present in *GRL* with an index I_D close to the candidate one (e.g. differing less than 5%) are selected, resulting in an ordered sublist $GRL_D \subseteq GRL$; if none is found, the candidate configuration is inserted into *GRL* using I_D as ordering criterion and the processing of the current grasp candidate ends.
2. All grasp configurations of GRL_D with an index I_E close to the candidate one (e.g. differing less that 10%) are selected, resulting in an ordered sublist $GRL_E \subseteq GRL_D$; if none is found, the candidate configuration is inserted into GRL_D using I_E as ordering criterion and the processing of the current grasp candidate ends.
3. The candidate configuration is inserted into GRL_E using I_C as ordering criterion.

At the end of the process, *GRL* contains an ordered list of the best potential grasp configurations that have been ranked using I_D as main, but not rigid, ordering criteria. In fact, all the configurations with similar value of I_D turn out to be ordered with respect to the index I_E, while all the configurations with similar value of I_E turn out to be ordered with respect to the index I_C.

Whenever required, to reduce the computation time, a maximum number of the best grasp configurations to be held in *GRL*, e.g. 20–50, can be imposed without losing accuracy in the ranking criteria (only the number of best selected grasp candidates is reduced).

After this first selection, starting from the best ranked grasp, computationally expensive indices are evaluated only for a limited number of grasp configurations. First of all, a force closure test is applied: if the evaluated grasp is not force closure, the next grasp of the list is considered, otherwise the grasp isotropy index I_G is evaluated and compared to a suitable acceptability threshold. If the grasp does not present a good value of I_G, the next grasp of the list is considered, otherwise the hand and task kinematic indices are evaluated to accept or discard the grasp. Finally, the reachable tests of each selected grasp region, as well as for the whole hand, are applied to the current best candidate until a good candidate is found. A grasp configuration exceeding all the tests is classified as the best feasible grasp and the process ends.

Notice that if, during the selection process, none of the n-fingered grasp configurations is suitable, the number of fingers can be reduced. This may happen when the object shape and size do not allow a suitable grasp with n fingers or when the grasp configurations resulting after the first step are discarded by the final validation tests (i.e. when the force-closure test or the reachable test fails, as well as when the grasp isotropy index is lower than the chosen threshold).

4. Case studies

Different case studies in 2D and 3D have been considered to evaluate the performance of the proposed algorithm. The proposed

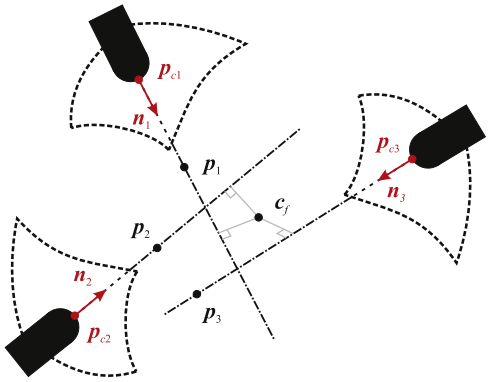

Fig. 7. Point at minimum distance form the action lines of the normal vectors at the contact points.

algorithm is applied first to a variety of cases to demonstrate its effectiveness. Then, a comparison with the results achieved with other approaches is proposed.

The main objective of this method is the synthesis of grasp configurations which are isotropic with respect to the center of mass of the object. In ideal conditions, the normal vectors at the contact points should have a uniform angular distribution and point to the center of mass of the object. In real cases, the angular distribution is not uniform, the normal vectors do not necessarily intersect in a common point and/or the intersection point is different from the center of mass.

To check the uniformity of the angular distribution of the normal vectors, the measure defined as "arrangement of force directions" in [4] can be computed as

$$\Delta\varphi = \frac{1}{n}\sum_{i=1}^{n}\left|\theta_i - \frac{2\pi}{n}\right|, \tag{7}$$

where θ_i is the angle between the normal vectors for two successive points of the grasp polygon.

The off-centering of the system of forces can be evaluated as $\boldsymbol{c}_m - \boldsymbol{c}_f$, where $\boldsymbol{c}_f$ is the point at minimum distance from the action lines of the normal vectors computed as

$$\boldsymbol{c}_f = \min_{\boldsymbol{p}} \sum_{i=1}^{n} \mathrm{d}(\boldsymbol{p}, l_n(\boldsymbol{p}_{ci})), \tag{8}$$

where $\mathrm{d}(\boldsymbol{p}, l_n(\boldsymbol{p}_{ci}))$ is the distance between the point $\boldsymbol{p}$ and the line $l_n(\boldsymbol{p}_{ci})$, which is the line of action of the normal vector to the surface in the contact point $\boldsymbol{p}_{ci}$ (see Fig. 7).

4.1. 2D case study

A 2D case is first considered on a variety of object shapes. After the grasp regions extraction and the grasp synthesis, an analysis of the grasp stability, the computational complexity, and the comparison with other methods are proposed.

4.1.1. Grasp region evaluation

The object reported in Fig. 8 is considered, with a maximum dimension of about 15 cm and a uniform mass distribution. The object is represented with ordered sets of connected points of its contours (for the shown example it has been employed about 1000 sampling points). On the top-right of the figure, the minimal inertia regions $\mathcal{R}_I$ are shown, assuming a friction coefficient $\mu = 0.4$. The red parts denote the selected regions while the regions in yellow are minimal inertia regions discarded due to their insufficient size with respect to the considered fingertip size, inaccessibility or excessive curvature. The center of mass $\boldsymbol{c}_m$ is represented with the blue plus symbol. On the bottom-right of the figure, the resulting grasp regions $\mathcal{R}_G$ are shown using alternatively black and green color to distinguish adjacent regions.

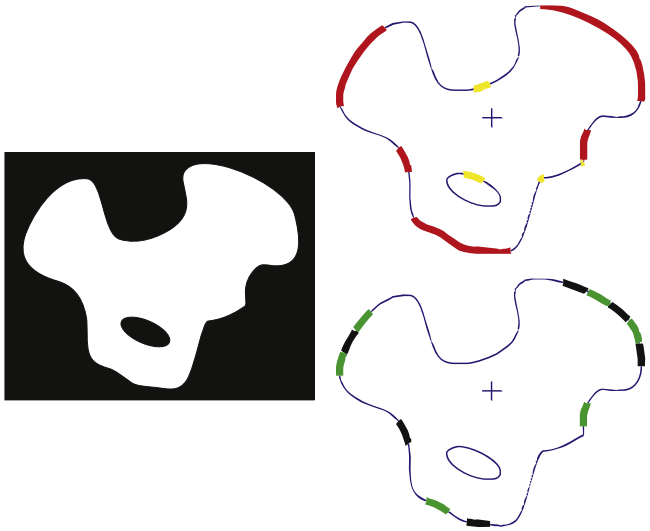

Fig. 8. Minimal inertial regions (top-right) and grasp regions (bottom-right) of the object shown on the left.

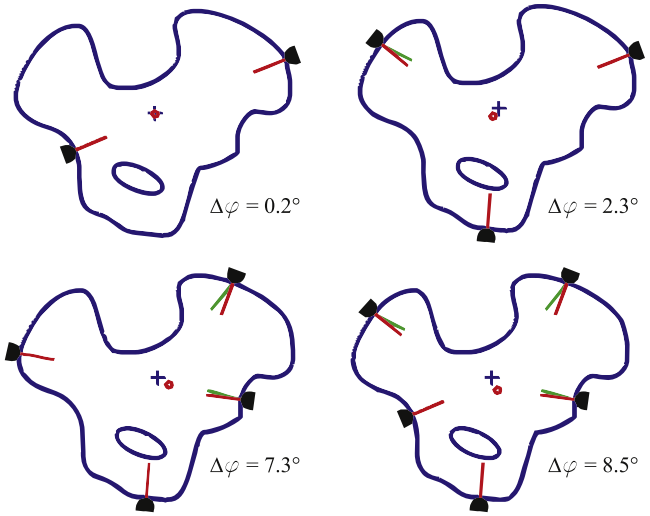

Fig. 9. Best grasp configurations for the object of Fig. 8 in the cases of $n = 2, \ldots, 5$ fingers.

4.1.2. Grasp synthesis

The best grasp configuration for the case of n fingers, with $n = 2, \ldots, 5$, and the object of Fig. 8 are shown in Fig. 9. On the bottom-right of each figure is reported the measure $\Delta\varphi$; also, the positions of $\boldsymbol{c}_m$ (blue plus symbol) and $\boldsymbol{c}_f$ (red circle symbol) are reported. Moreover, at each contact point, the normal vector (red line) and the central vector (green line) are reported; when these vectors are aligned, only the red vector is visible. Notice that the value of $\Delta\varphi$ increases with n, as well as the distance between $\boldsymbol{c}_m$ and $\boldsymbol{c}_f$; in fact, for the given number of grasp regions in $\mathcal{R}_G$, finding isotropic configurations centered at $\boldsymbol{c}_m$ becomes more difficult.

To evaluate the capability of the algorithm to ensure the synthesis of grasp configurations that minimize the gravitational and inertial effects, two different mass distributions are considered in Fig. 10 for a 3-fingered grasp. In both cases, two of the three fingers tend to be close to the center of mass, favoring the compensation of gravitational effects.

4.1.3. Stability analysis

To test the stability of the proposed algorithm – i.e., the invariance of the solution with respect to minimal deformation of

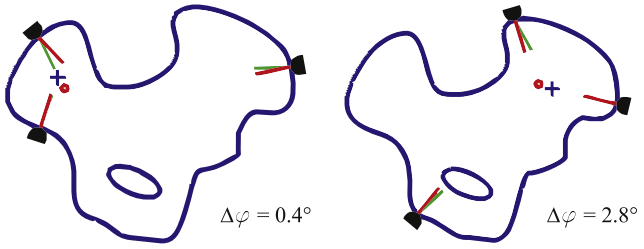

Fig. 10. Best 3-fingered grasp configurations for the object of Fig. 8 in the case of two different mass distributions.

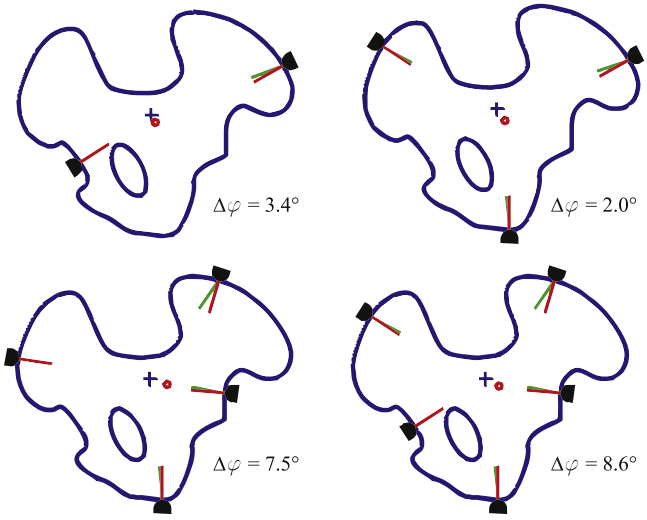

Fig. 11. Best grasp configurations for a deformed version of the object of Fig. 8.

the object – a deformed version of the object of Fig. 8 has been processed. The results are reported in Fig. 11, where the substantial invariance of the configurations with respect to those reported in Fig. 9, can be appreciated.

4.1.4. Computational complexity

The required computation time for the proposed algorithm depends of the shape and size of the object, and of the number of desired fingertips. For all the objects considered here, using 1000 sample points for the object borders, the computation times using a C++ code on a Pentium at 2.8 GHz is about 14 ms in the case of 2 fingers, 16 ms for 3 fingers, 19 ms for 4 fingers, and 24 ms for 5 fingers.

4.1.5. Comparison with other methods

An explicit comparison with the results of other methods proposed in the literature has been carried out. In Fig. 12 the best grasps for two objects considered in [23] are shown, using our method (black filled half-circles) and the method in [23] (red filled circles).

For the object on the left, the two best grasps computed with our algorithm correspond to their two best ones, but in an inverted order. The arrangement of force directions for the proposed method is $\Delta\varphi = 31.9°$, while for the best grasp proposed in [23] is $\Delta\varphi = 41.6°$, which corresponds to an improvement of 23.3%. The ratio between the off-centering of the best grasp evaluated in [23] and that achieved with our method is 3.7 corresponding to a relative improvement of 73%.

For the object on the right, our best grasp does not correspond to any of the best six ones shown in [23], but it is quite evident that our grasp is quite natural and effective. In fact, the best grasp computed in [23] requires that one finger acts a force outgoing

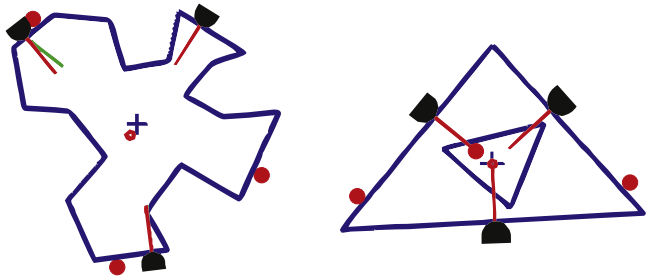

Fig. 12. Best 3-fingered grasp configurations for two objects considered in [23] (red discs represent the best grasps evaluated with the method proposed in [23]). (For interpretation of the references to colour in this figure legend, the reader is referred to the web version of this article.)

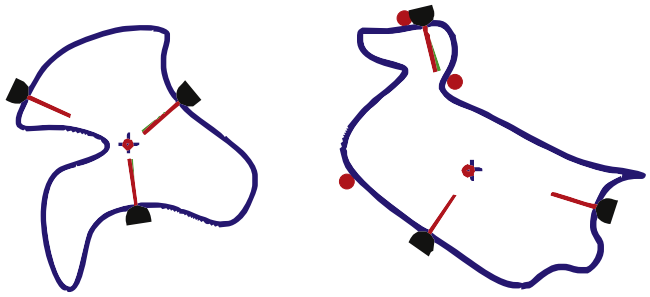

Fig. 13. Best 3-fingered grasp configurations for two objects considered in [21] (red discs represent the best grasps evaluated with the method proposed in [21]). (For interpretation of the references to colour in this figure legend, the reader is referred to the web version of this article.)

with respect to the center of the object, and this can represent an issue for many robotic hands. Moreover, the arrangement of force directions are $\Delta\varphi = 15.1°$ and $\Delta\varphi = 14°$, respectively. In this case, the reduction is limited due to the geometrical conformation of the object, which is quite constrained in the selection of the applied force direction. On the other hand, the off-centering of the proposed method is zero, while it is not so in [23].

In Fig. 13 the best grasps for two objects considered in [21] are shown, using our method (black filled half-circles) and the method in [21] (red filled circles). For the object on the left, the same identical best grasp is achieved, while for the object on the right, our best grasp does not correspond to those evaluated in [21], but again our grasp seems to be natural and effective. In fact, though $\Delta\varphi = 2.1°$ in [21] while $\Delta\varphi = 8.7°$ for our method, which could be considered both to be very good, the ratio between the off-centerings is 24.3, which corresponds to a relative improvement of 96%.

Notice that, since the methodology and the quality indices adopted in the papers considered for the previous comparisons are different from the ones adopted in this work, which are focused on the dynamic consistency of the grasp, the achieved results cannot surprise. Nevertheless, the authors consider this explicit comparison worthy, for example to underline the fact that the proposed dynamically consistent approach does not penalize other important quality factors to achieve a stable and optimal grasp configuration.

4.2. 3D case study

In this section three different CAD models of a duck-toy, a wine glass, and a shaped bottle are considered to demonstrate the feasibility and the effectiveness of the proposed approach in several conditions depending on the model resolution as well as on the number of employed fingers. An anthropomorphic 5-fingered hand is considered for the hand kinematic constraints test and for the

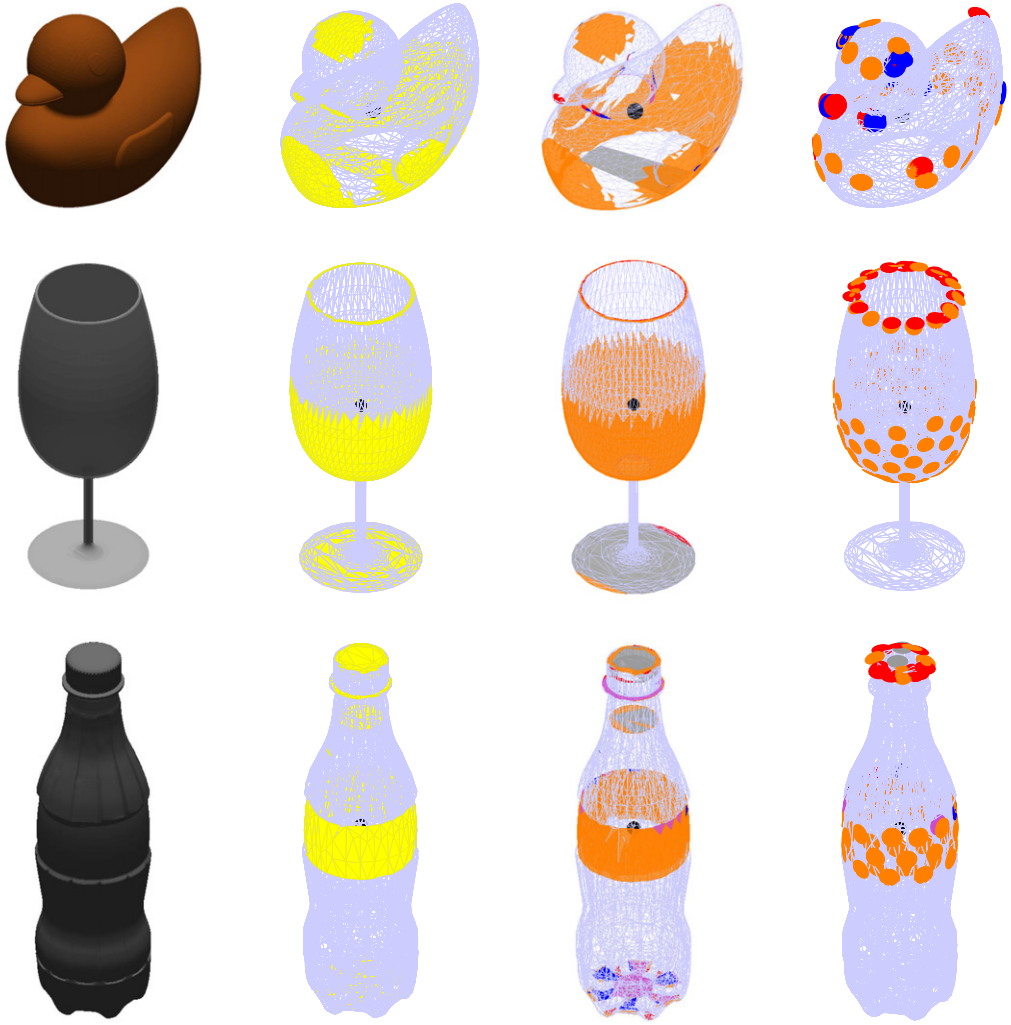

Fig. 14. From the left: the CAD models of the objects employed in the 3D case studies and the corresponding minimal inertia regions (yellow), the uniform curvature regions (planar regions in gray, convex regions in orange, concave regions in violet, convex corner regions in red, and concave corner regions in blue), and the grasp regions (discs with the fingertips size and the same color convention adopted for the uniform curvature regions). The black sphere indicates the center of gravity. (For interpretation of the references to colour in this figure legend, the reader is referred to the web version of this article.)

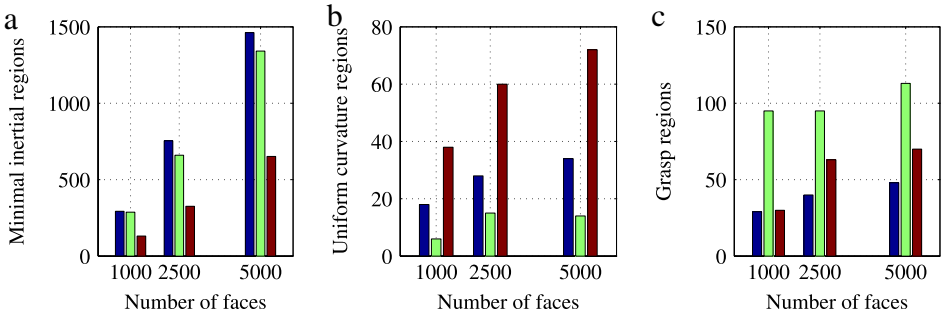

Fig. 15. Number of the minimal inertial regions (a), of the uniform curvature regions (b), and of the grasp regions (c) extracted from the CAD models of the duck-toy (blue), of the wine glass (green), and of the shaped bottle (red) with three different resolution (triangle mesh with 1000, 2500, and 5000 faces, respectively). (For interpretation of the references to colour in this figure legend, the reader is referred to the web version of this article.)

hand kinematic grasp quality index. The size of the hand is the human one, with a maximum grasp extension between the thumb and the other fingers limited to 12 cm. The friction coefficient and all the other main parameters are similar to the 2D case for all the objects.

Triangle meshes with three different resolutions for each single object have been used, i.e. 1000, 2500, and 5000 faces, respectively. These last values are apparently too large with respect to the dimensions of the employed fingers and objects. However, one of the purposes of this section is the evaluation of the performance of the proposed approach, hence such large values clearly allow drawing the trend in the computation time and complexity of the algorithm.

4.2.1. Grasp regions evaluation

The CAD models of the employed object (a duck-toy, a wine glass, and a shaped bottle) are shown in Fig. 14 together with

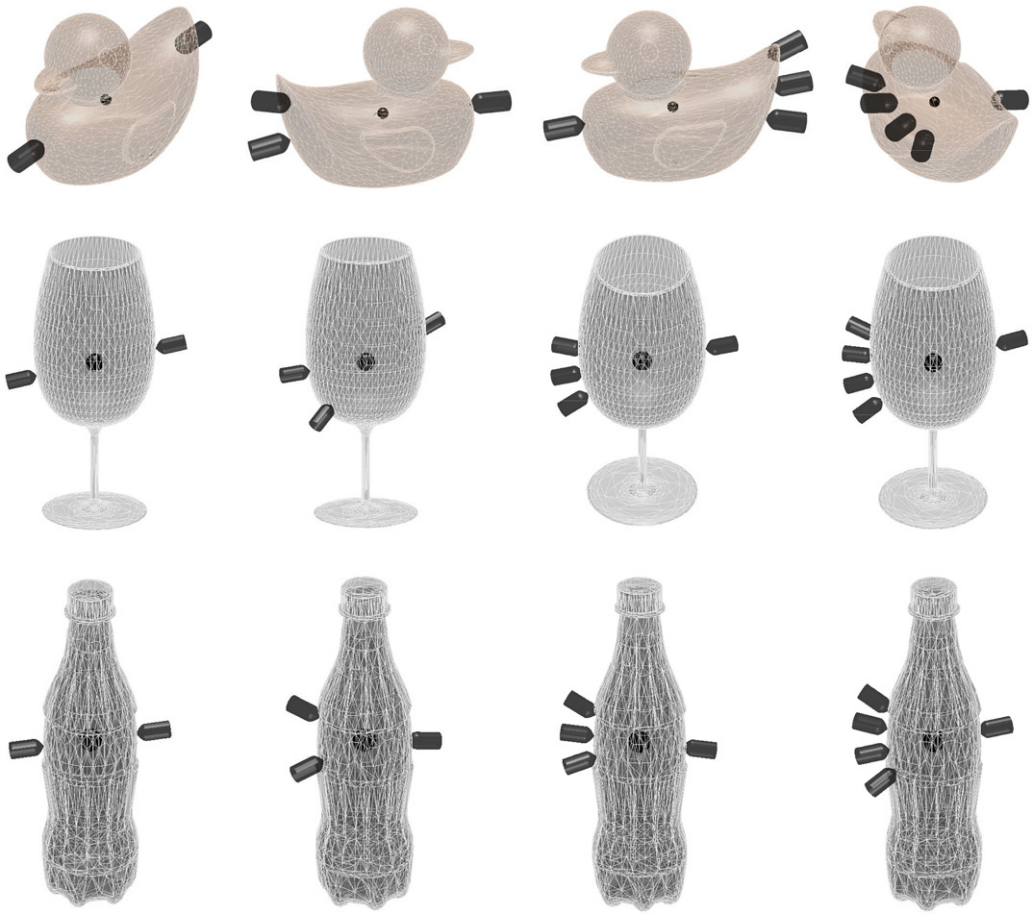

Fig. 16. Best-ranked grasp configurations for the objects of Fig. 14 with $n = 2, \ldots, 5$ fingers (from the left to the right). The black sphere indicates the center of gravity.

the corresponding minimal inertia regions, the uniform curvature regions, and the grasp regions. In particular, the duck-toy is 10 cm high, the wine glass is 18 cm high, and the shaped bottle is 18 cm high.

Fig. 15 shows the number of minimal inertial regions, of the uniform curvature regions, and of the grasp regions extracted from the CAD models of the employed objects by using triangle meshes with three different resolutions (1000, 2500, and 5000 faces). The dimension of $\mathcal{R}_I$ increases almost linearly with the resolution of the meshes (see Fig. 15(a)), as it was expected. On the other hand, the dimensions of $\mathcal{R}_C$ and of $\mathcal{R}_G$ increase with a sublinear rate (see Fig. 15(b) and (c)). This last behavior is expected because, by increasing the mesh resolution, the dimensions of $\mathcal{R}_C$ and of $\mathcal{R}_G$ (being fixed the fingertip dimension) have to become constant.

4.2.2. Grasp synthesis

The best-ranked grasp configurations for the objects of Fig. 14 are shown in Fig. 16 for the cases of $n = 2, \ldots, 5$. It is worth noticing how, depending on the dimension and shape of the object, the best grasp configurations by changing the number of fingers employed for the grasp are very similar. This result is a demonstration of the numerical stability of the proposed algorithm.

The minimization of the gravitational effects has been tested by considering the cases of an half-filled bottle, i.e. by modifying the position of the center of gravity of the bottle with respect to the case shown before. The corresponding best-ranked grasp configurations are shown in Fig. 17 for $n = 2, \ldots, 5$. In all cases, the off-centering of the line of action of the applied fingertips forces is negligible, and then the compensation of gravitational effects is maximized.

4.2.3. Computational complexity

The computational complexity of the proposed approach in the 3D case has been evaluated by measuring the time needed for the grasp synthesis of the best grasp configuration for the objects of Fig. 14 with different triangle-mesh resolution. An Intel Pentium processor at 2.8 GHz with a C++ code has been employed.

First, the computation time required for the extraction of the minimal inertial regions, uniform curvature regions, and grasp regions are shown in Fig. 18. A linear increasing trend with respect to the object model resolution is clearly evidenced for this step, as it was expected. In any case, the required time intervals are reasonably low and widely compatible with on-line computation.

On the other hand, the total computation times required for the optimal grasp synthesis with respect to the number of employed fingers are shown in Fig. 19. For all the employed objects (a duck-toy, a wine glass, and a shaped bottle), the computation time increase with respect to the number of fingers with a sublinear rate. The worst case corresponds to the wine glass object (Fig. 19(b)). The reasons for these results are at least two: (1) the number of grasp regions is higher than in the other cases; (2) many of the best-ranked grasp regions for $n = 3, 4$ turn out to be unsuitable after the post elaboration tests (mainly due to the whole-hand reachability test that fails for size and dimension of the object) that are applied in sequence, until a suitable grasp configuration is found. This last case represents also the most significant drawback of the proposed approach, i.e. when several

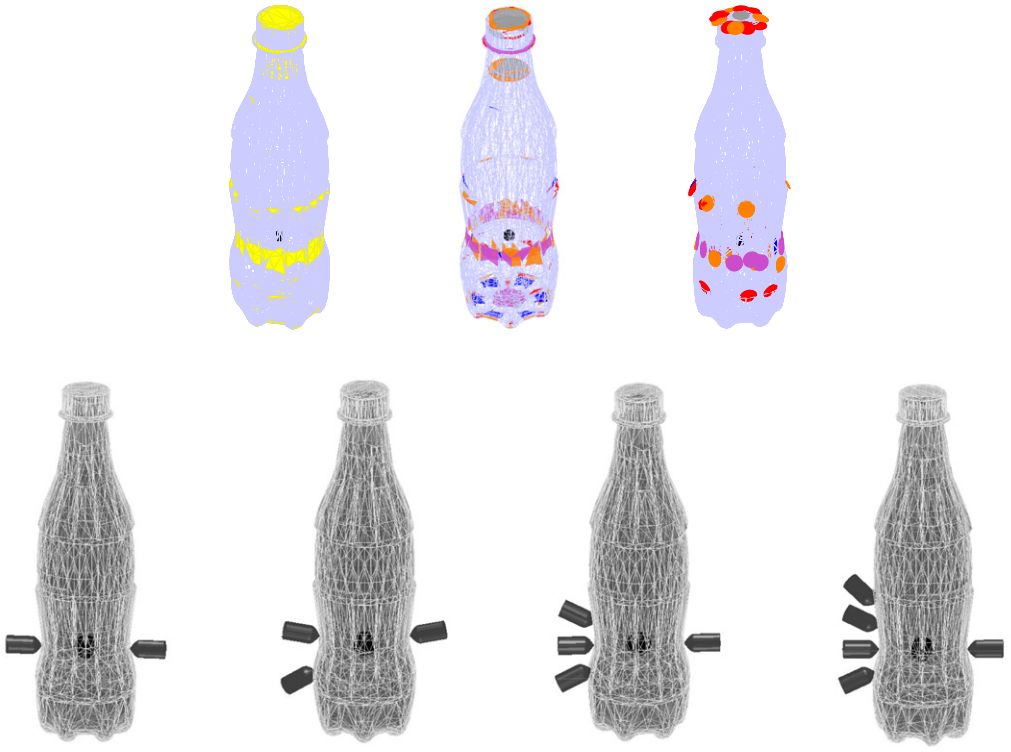

Fig. 17. Best-ranked grasp configurations for the half-filled shaped bottle, i.e. when an offset is applied to the center of gravity.

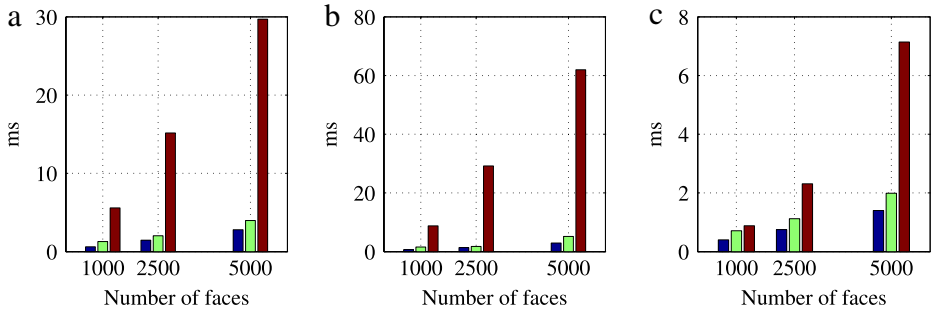

Fig. 18. Computation times required for the selection of the minimal inertial regions (blue), for the uniform curvature regions (green), and for the grasp regions (red) from the CAD models of the duck-toy (a), of the wine glass (b), and of the shaped bottle (c) with three different resolutions (triangle mesh with 1000, 2500, and 5000 faces, respectively). (For interpretation of the references to colour in this figure legend, the reader is referred to the web version of this article.)

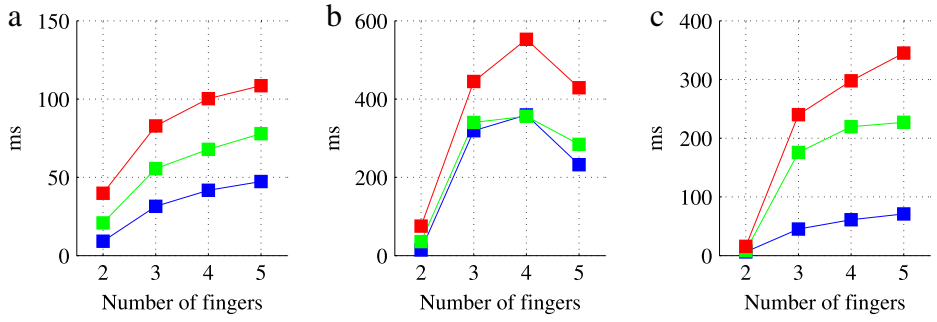

Fig. 19. Total computation times required for the evaluation of the best grasp configurations with a number of fingers $n = 2, \ldots, 5$ and for different CAD model resolutions (1000 faces in blue, 2500 faces in green, and 5000 faces in red). Three different objects are considered: (a) duck-toy, (b) wine glass, and (c) shaped bottle. (For interpretation of the references to colour in this figure legend, the reader is referred to the web version of this article.)

best-ranked grasp configurations are discarded before a suitable grasp is found. This kind of test being time consuming, the total computation time then increases. However, also in this case, the required computational time makes the proposed technique applicable for on-line computation of grasps.

5. Conclusion

In this paper the problem of finding grasp configurations which reduce the gravitational and inertial effects of the object on the hand has been addressed. A new method for fast synthesis of multi-

fingered grasp configurations has been proposed. A number of case studies both in 2D and in 3D, as well as comparisons with other methods have been presented showing the effectiveness of the proposed approach. In particular, in all the considered examples, the proposed method allows either computing the same grasps as those of other approaches that are far more computational expensive, or to achieve alternative grasps which are suitable for manipulating heavy objects.

References

[1] W. Howard, V. Kumar, On the stability of grasped objects, IEEE Transactions on Robotics and Automation 12 (6) (1996) 904–917.
[2] A. Bicchi, On the closure properties of robotic grasping, International Journal of Robotics Research 14 (1995) 319–334.
[3] A. Okamura, N. Smaby, M. Cutkosky, An overview of dexterous manipulation, in: IEEE International Conference on Robotics and Automation, Vol. 1, 2000, pp. 255–262.
[4] Y. Park, G. Starr, Optimal grasping using a multifingered robot hand, in: IEEE International Conference on Robotics and Automation, 1990, pp. 689–694.
[5] V. Lippiello, B. Siciliano, L. Villani, A grasping force optimization algorithm for multi-arm robots with multi-fingered hands, IEEE Transactions on Robotics 29 (1) (2013) 55–67.
[6] V. Lippiello, B. Siciliano, L. Villani, A grasping force optimization algorithm for dexterous robotic hands, in: IEEE International Conference on Robotics and Automation, 2012, pp. 4170–4175.
[7] T. Watanabe, T. Yoshikawa, Grasping optimization using a required external force set, IEEE Transactions on Automation Science and Engineering 4 (1) (2007) 52–66.
[8] L. Ying, J. Fu, N. Pollard, Data-driven grasp synthesis using shape matching and task-based pruning, IEEE Transactions on Visualization and Computer Graphics 13 (4) (2007) 732–747.
[9] K. Shimoga, Robot grasp synthesis algorithms: a survey, The International Journal of Robotics Research 15 (3) (1996) 230–266.
[10] A. Sahbani, S. El-Khoury, P. Bidaud, An overview of 3D object grasp synthesis algorithms, Robotics and Autonomous Systems 60 (3) (2012) 326–336.
[11] D. Prattichizzo, J.C. Trinkle, Grasping, in: B. Siciliano, O. Khatib (Eds.), Springer Handbook of Robotics, Springer, Berlin, Heidelberg, 2008, pp. 671–700 (Chapter 28).
[12] J. Aleotti, S. Caselli, A 3D shape segmentation approach for robot grasping by parts, Robotics and Autonomous Systems 60 (3) (2012) 358–366.
[13] V. Lippiello, F. Ruggiero, B. Siciliano, L. Villani, Visual grasp planning for unknown objects using a multifingered robotic hand, IEEE/ASME Transactions on Mechatronics 18 (3) (2013) 1050–1059.
[14] V. Lippiello, F. Ruggiero, B. Siciliano, L. Villani, Preshaped visual grasp of unknown objects with a multi-fingered hand, in: IEEE/RSJ International Conference on Intelligent Robots and Systems, 2010, pp. 5894–5899.
[15] J.-P. Saut, D. Sidobre, Efficient models for grasp planning with a multi-fingered hand, Robotics and Autonomous Systems 60 (3) (2012) 347–357.
[16] R. Suárez, M. Roa, J. Cornella, Grasp quality measures, Tech. Rep., Technical University of Catalonia, 2006.
[17] A. Bicchi, V. Kumar, Robotic grasping and contact: a review, in: IEEE International Conference on Robotics and Automation, Vol. 1, 2000, pp. 348–353.
[18] B.-H. Kim, S.-R. Oh, B.-J. Yi, I.H. Suh, Optimal grasping based on non-dimensionalized performance indices, in: IEEE/RSJ International Conference on Intelligent Robots and Systems, Vol. 2, 2001, pp. 949–956.
[19] B.-H. Kim, B.-J. Yi, S.-R. Oh, I.H. Suh, Non-dimensionalized performance indices based optimal grasping for multi-fingered hands, Mechatronics 14 (3) (2004) 255–280.
[20] Z. Li, S. Sastry, Task-oriented optimal grasping by multifingered robot hands, IEEE Journal of Robotics and Automation 4 (1) (1988) 32–44.
[21] E. Chinellato, A. Morales, R. Fisher, A. del Pobil, Visual quality measures for characterizing planar robot grasps, IEEE Transactions on Systems, Man, and Cybernetics Part C: Applications and Reviews 35 (1) (2005) 30–41.
[22] R. Hester, M. Cetin, C. Kapoor, D. Tesar, A criteria-based approach to grasp synthesis, in: IEEE International Conference on Robotics and Automation, Vol. 2, 1999, pp. 1255–1260.
[23] J. Ponce, B. Faverjon, On computing three-finger force-closure grasps of polygonal objects, IEEE Transactions on Robotics and Automation 11 (6) (1995) 868–881.
[24] C.-P. Tung, A. Kak, Fast construction of force-closure grasps, IEEE Transactions on Robotics and Automation 12 (4) (1996) 615–626.
[25] D. Ding, Y.-H. Lee, S. Wang, Computation of 3-D form-closure grasps, IEEE Transactions on Robotics and Automation 17 (4) (2001) 515–522.
[26] Y. Park, G. Starr, Grasp synthesis of polygonal objects, in: IEEE International Conference on Robotics and Automation, 1990, pp. 1574–1580.
[27] M. Roa, R. Suarez, Geometrical approach for grasp synthesis on discretized 3D objects, in: IEEE/RSJ International Conference on Intelligent Robots and Systems, 2007, pp. 3283–3288.
[28] K. Charusta, R. Krug, D. Dimitrov, B. Iliev, Independent contact regions based on a patch contact model, in: IEEE International Conference on Robotics and Automation, 2012, pp. 4162–4169.
[29] V. Lippiello, B. Siciliano, L. Villani, Fast multi-fingered grasp synthesis based on object dynamic properties, in: IEEE/ASME International Conference on Advanced Intelligent Mechatronics, 2010, pp. 1134–1139.
[30] D. Montana, The condition for contact grasp stability, in: IEEE International Conference on Robotics and Automation, 1991, pp. 412–417.
[31] J. Ponce, S. Sullivan, A. Sudsang, J.-D. Boissonnat, J.-P. Merlet, On computing four-finger equilibrium and force-closure grasps of polyhedral objects, International Journal of Robotics Research 16 (1996) 11–35.
[32] E. Chinellato, R. Fisher, A. Morales, A. del Pobil, Ranking planar grasp configurations for a three-finger hand, in: IEEE International Conference on Robotics and Automation, Vol. 1, 2003, pp. 1133–1138.
[33] B. Mirtich, J. Canny, Easily computable optimum grasps in 2-D and 3-D, in: IEEE International Conference on Robotics and Automation, 1994, pp. 739–747.
[34] Y. Li, Q. Meng, S. Tso, An approach to dynamic grasp stability measurement, in: IEEE Instrumentation and Measurement Technology Conference, Vol. 2, 1998, pp. 1168–1173.
[35] C.-H. Xiong, Y.-F. Li, H. Ding, Y.-L. Xiong, On the dynamic stability of grasping, The International Journal of Robotics Research 18 (9) (1999) 951–958.
[36] R.M. Murray, S.S. Sastry, L. Zexiang, A Mathematical Introduction to Robotic Manipulation, first ed., CRC Press, Inc., Boca Raton, FL, USA, 1994.
[37] S. El-Khoury, A. Sahbani, On computing robust *n*-finger force-closure grasps of 3D objects, in: IEEE International Conference on Robotics and Automation, 2009, pp. 2480–2486.

V. Lippiello was born in Naples, Italy, on June 19, 1975. He received his Laurea degree in electronic engineering and Research Doctorate degree in information engineering from the University of Naples, Naples, Italy, in 2000 and 2004, respectively. He is an Assistant Professor of Automatic Control in the Department of Computer and Systems Engineering, University of Naples. His research interests include visual servoing of robot manipulators, hybrid visual/force control, adaptive control, grasping and manipulation. He has published more than 60 journal and conference papers and book chapter. He is chair of the IFAC Technical Committee on Robotics.

B. Siciliano (M'91-SM'94-F'00) was born in Naples, Italy, on October 27, 1959. He received his Laurea degree and Research Doctorate degree in Electronic Engineering from the University of Naples in 1982 and 1987, respectively. He is Professor of Control and Robotics, and Director of the PRISMA Lab in the Department of Computer and Systems Engineering at University of Naples. He has coauthored 7 books, 70 journal papers, 180 conference papers and book chapters; his book Robotics: Modelling, Planning and Control is one of the most widely adopted textbooks world-wide. He has delivered 100 invited lectures and seminars at institutions worldwide.

He is a Fellow of IEEE, ASME and IFAC. He is Co-Editor of the Springer Tracts in Advanced Robotics series, and has served on the Editorial Boards of several journals as well as Chair or Co-Chair for numerous international conferences.

He co-edited the Springer Handbook of Robotics, which received the PROSE Award for Excellence in Physical Sciences and Mathematics and was also the winner in the category Engineering and Technology.

He has been the coordinator of the large-scale integrating project DEXMART on dexterous and autonomous dual-arm/hand manipulation, funded by the European Commission in the 7th Framework Programme, and his group is currently involved in another five FP7 projects.

He has served the IEEE Robotics and Automation Society as Vice-President for Technical Activities and Vice-President for Publications, as a member of the AdCom, as a Distinguished Lecturer, and as the Society President.

L. Villani (S'94-M'97-SM'03) was born in Avellino, Italy, on December 5, 1966. He received his Laurea degree in electronic engineering and Research Doctorate degree in electronic engineering and computer science from the University of Naples, Naples, Italy, in 1992 and 1996, respectively. He is an Associate Professor of Automatic Control in the Department of Computer and Systems Engineering, University of Naples. His research interests include force/motion control of manipulators, cooperative robot manipulation, lightweight flexible arms, adaptive and nonlinear control of mechanical systems, visual servoing, fault diagnosis, and fault tolerance for dynamical systems. He has coauthored 5 books, 40 journal papers and 100 conference papers and book chapters.

Dr. Villani was Associate Editor of IEEE Transactions on Robotics from 2007 to 2011 and he is Associate Editor of IEEE Transactions on Control Systems Technology from 2005.